Supporting Information

Methanol to Olefins Reaction Route Based on Methylcyclopentadienes as Critical Intermediates

Wenna Zhang,[†, §, ⊥] Yuchun Zhi,[†, ⊥] Jindou Huang,[†] Xinqiang Wu,[†] Shu Zeng,[†, §] Shutao Xu,[†] Anmin Zheng, [‡,∥,*] Yingxu Wei, [†,*] Zhongmin Liu[†,*]

† National Engineering Laboratory for Methanol to Olefins, Dalian National Laboratory for Clean Energy, iChEM (Collaborative Innovation Center of Chemistry for Energy Materials), Dalian Institute of Chemical Physics, Chinese Academy of Sciences, Dalian 116023, P. R. China

‡ State Key Laboratory of Magnetic Resonance and Atomic Molecular Physics, National Center for Magnetic Resonance in Wuhan, Institute of Physics and Mathematics, Chinese Academy of Sciences, Wuhan 430071, P. R. China

§University of Chinese Academy of Sciences, Beijing 100049, P. R. China

∥School of Materials Science and Engineering, Zhengzhou University, Zhengzhou, Henan 450052, P. R. China

*E-mail: liuzm@dicp.ac.cn (Z. Liu)

weiyx@dicp.ac.cn (Y. Wei)

zhenganm@wipm.ac.cn (A. Zheng)

Table of Contents

1. Catalyst Characterizations

1.1 Material

H-SAPO-34 （Si/(Si+Al+P)=0.09） was synthesized following the procedure described in the literature.[1] The H-SAPO-34 was obtained by calcination of the crystallized products at 550 °C for 4 h.

1.2 Powder X-ray Diffraction (XRD)

Powder X-ray diffraction (XRD) pattern of H-SAPO-34 was recorded on a PANalytical X'Pert PRO X-ray diffractometer equipped with Cu Kα radiation (λ = 0.15418 nm) from 5 and 40° with a scan speed of 2θ =5.0 °/min at 40 kV and 40 mA. The reflection peaks are in good agreement with the standard sample and no other impurity phases were observed as presented in **Figure S1**.
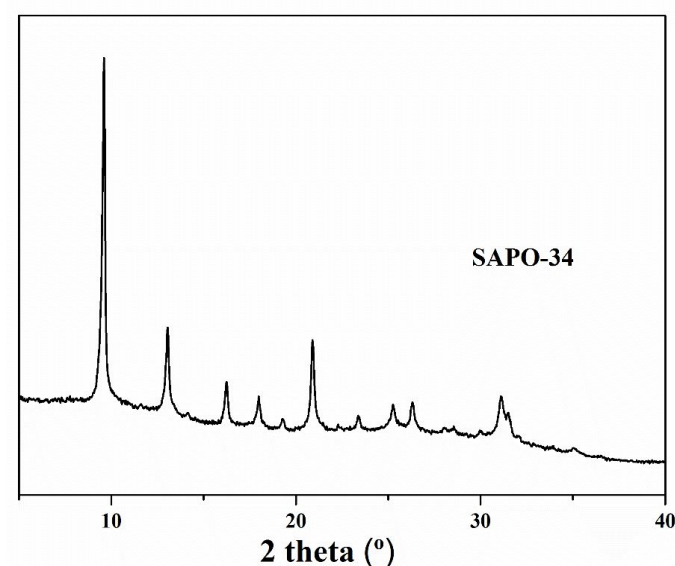

Figure S1. XRD pattern of SAPO-34 sample.

1.3 Scanning Electron Microscopy (SEM)

To investigate the crystal size and morphology of H-SAPO-34 catalyst, a HITACHI SU8020 Scanning Electron Microscope was employed.
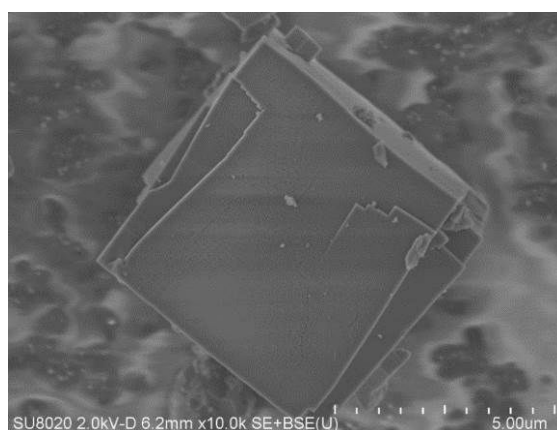

Figure S2. SEM image of H-SAPO-34 sample.

2. Experimental Section and Theoretical Calculation

2.1 Methanol to Olefin Conversion

MTO reaction was performed in a fixed-bed quartz tubular reactor under atmospheric pressure. Prior to reaction, the SAPO-34 catalysts were firstly calcined under air atmosphere at 550 °C for 4 h to remove the organic template. Then the calcined catalysts were loaded into the reactor and activated in helium flow at 500 °C for 1 h. The methanol was fed by passing the carrier gas (He) through a methanol saturation evaporator maintained at 14 °C with the molar ratio of helium to methanol of 10 and WHSV of methanol of 2.0 h^{-1}. The effluent products were analyzed on online by gas chromatography (Agilent GC 7890A) equipped with a HP-PLOT Q capillary column and a FID detector.

2.2 ^{13}C MAS NMR Spectroscopy

For the ^{13}C MAS NMR spectroscopy measurement of the retained organics in the catalyst, methanol conversion was performed with ^{13}C-methanol as the reactant. ^{13}C-methanol was fed into the reactor for 10 min and then the reactor was removed from the feeding line, and the catalyst was cooled very quickly by putting them into the vessel containing liquid nitrogen. Finally, the cooled catalyst was transferred to an NMR rotor in the glove box without exposure to ambient air.

All the solid-state ^{13}C MAS NMR measurements were performed on a Bruker AvanceIII 600 spectrometer equipped with a 14.1 T wide-bore magnet using a 4 mm MAS probe. The resonance frequency was 150.9 MHz for ^{13}C nucleus. ^{13}C MAS NMR spectra were recorded using high-power proton decoupling with a spinning rate of 12 kHz. A 2700 scans were accumulated with a π/4 pulse width of 1.8 μs and a 4 s recycle delay. The chemical shifts were referenced to adamantane with the up field methine peak at 29.5 ppm.

2.3 ^{12}C/^{13}C-methanol Switch Experiment

In the ^{12}C/^{13}C-methanol switch experiment, the ^{12}C-methanol was fed by passing the carrier gas (He) through a methanol saturation evaporator maintained at 14 °C into the reactor at 300 °C for 25 min to build up ^{12}C-hydrocarbon pool species in the cavity of H-SAPO-34. Then the feeding of ^{12}C-methanol was stopped and ^{13}C-methanol (fed by passing the carrier gas (He) through a ^{13}C-methanol saturation evaporator) was switched into the reactor for 1 min and then the catalyst was cooled very quickly by putting them into the vessel containing liquid nitrogen. The isotopic distribution of effluents and the materials confined in the catalyst was analyzed using an Agilent 7890A/5975C GC/MSD.

2.4 Confined Organics Determination with GC−MS

Organic species trapped in the cages of SAPO-34 were analyzed following the procedures described in the literature by Guisnet.[2] After reaction, the spent catalysts were quickly cooled down to room temperature and then dissolved in 20% hydrofluoric acid solution. The organic phase was extracted by dichloromethane (CH_2Cl_2) with 120 ppm C_2Cl_6 as internal standard and then analyzed using an Agilent 7890A/5975C GC/MSD equipped with an HP-5 capillary column.

2.5 Confined Organics Confirmation by UV-vis

Ultraviolet–visible (UV–vis) spectra of spent catalysts were recorded on a VARIAN Cary-5000 UV–Vis–NIR spectrophotometer equipped with an integration sphere in the range of 200–800 nm. For each experiment, the same amount of catalyst and the same test conditions were used.

2.6 Theoretical Calculation Methods

For theoretical calculations, H-SAPO-34 was represented by an extended $74T(SiP_{36}Al_{37}O_{119}H_{59})$ cluster extracted from the crystallographic CHA structure, as shown in **Figures S3**. The locations of acid sites were chosen at the 8-MR window, accessible for adsorbents and surrounded by maximum reaction space.[3]
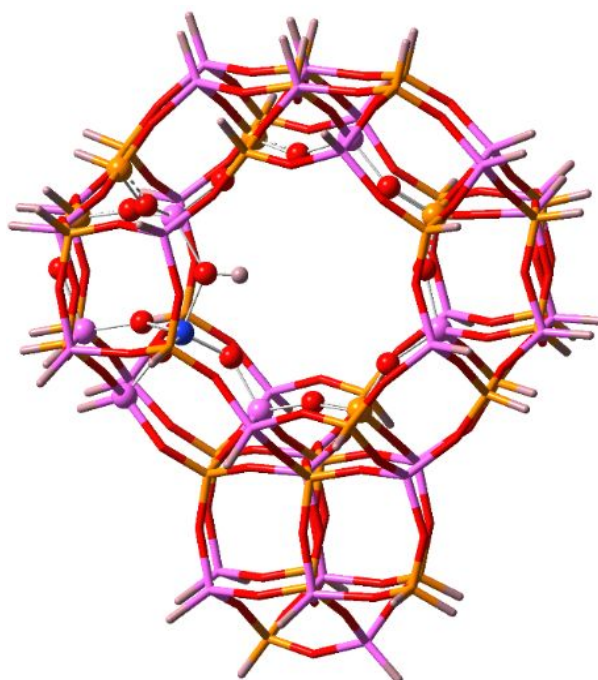

Figure S3. Representations of H-SAPO-34 framework structures by 74T cluster models. The ball and stick view is treated as the high-layer atoms during the ONIOM calculations.

The combined theoretical ONIOM method[4-6] was applied to predict the geometries of various adsorption structures and transition states (TS). During the structure optimization, ωB97XD hybrid density function with 6-31G (d, p) basis sets and semi-empirical AM1 were employed for optimizing geometries of the high-level layer and low-level layer. The ωB97XD method is the hybrid meta DFT developed by Chai and Head-Gordon, where implicitly accounts for empirical dispersion and can describe long-range dispersion interactions well with respect to the traditional DFT methods.[7] To preserve the integrity of the catalyst structure during the structure optimizations, the 8-MR window, $(SiO)_3$-Si-OH-Al-$(SiO)_3$ active center and the adsorbed species were in the high-level layer while the rest of atoms were in the low-level at their crystallographic locations. All the atoms except for the terminal H atoms were relax during the structure optimization. To obtain highly accurate energies, the single-point energies were calculated at the level of ωB97XD/6-31G(d, p) on the basis of optimized structures. The frequency calculations were performed at the same level as geometry optimizations to check whether the saddle points exhibit the proper number of imaginary frequencies. Only a single imaginary frequency was observed for the transition state, and no imaginary frequency was observed for the adsorbed state.

In order to compare with the real MTO reaction condition at 400 °C, the intrinsic free energies barriers ($\Delta G^{\ddagger}$) for each elementary reaction in a completed reaction route was obtained from the ωB97XD/6-31G (d, p) total electronic energies and the thermal correction from the ωB97XD/6-31G(d, p): AM1 frequency calculations. The

energies reported here have been corrected for zero-point vibration energies. All density functional theory (DFT) calculations were performed with the Gaussian 09 package.[8] The reaction rate constants were obtained through transition state theory (TST) as implemented in the TAMkin program,[9] which was developed in 2010.

3. Results and Discussion

3.1 Methanol to Olefins Conversion and Product Distribution over H-SAPO-34

The catalytic performances of methanol conversion over H-SAPO-34 at 300 $^{\circ}$C and 400 $^{\circ}$C are shown in **Figure S4 and S5**. An obvious induction period is observed at 300 $^{\circ}$C, with the increase of the temperature, complete methanol conversion is realized. Ethene and propene appear as the main products.
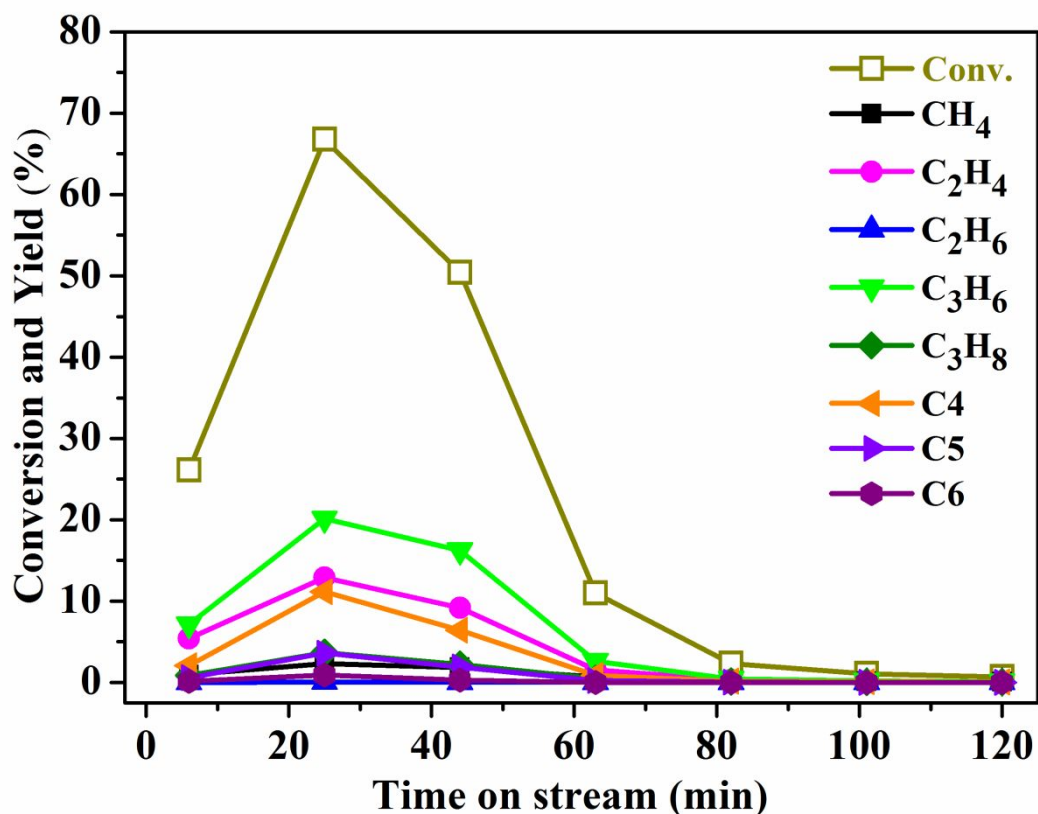

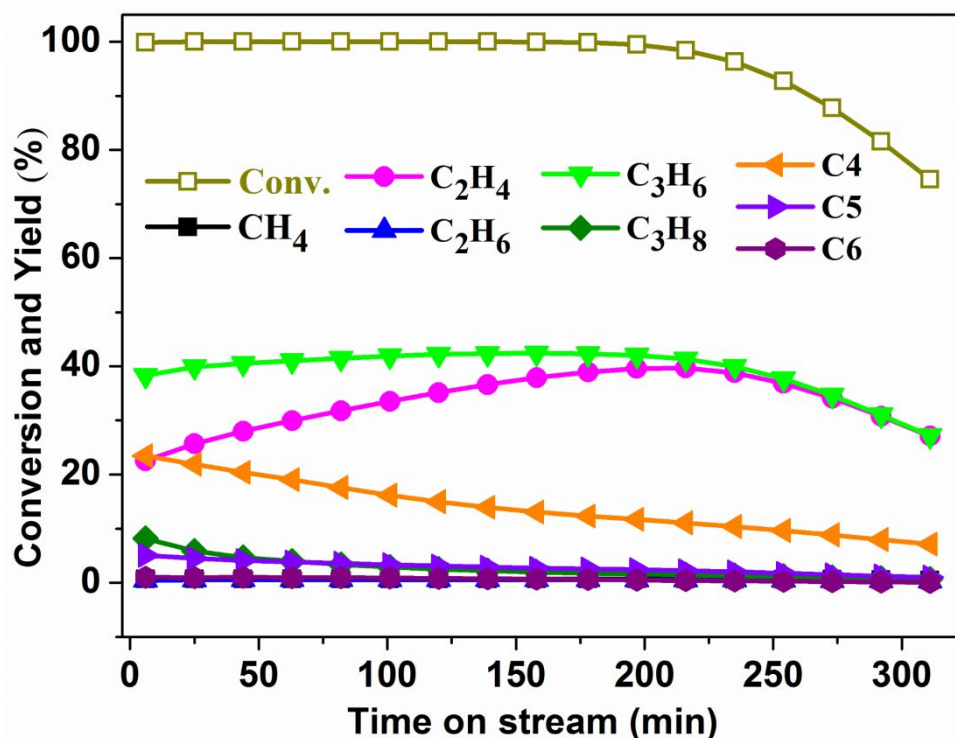**Figure S4.** Methanol conversion and hydrocarbon product yields over H-SAPO-34 catalyst with time on stream at 300 $^{\circ}$C.

Figure S5. Methanol conversion and hydrocarbon product yields over H-SAPO-34 catalyst with time on stream at 400 °C.

3.2 Identification of the Confined Carbenium Ions Using ^{13}C MAS NMR, GC-MS and UV-vis

The identification of the carbenium ions formed in H-SAPO-34 has been also consolidated by the GC-MS analysis of the confined organic species in the zeolite catalyst as shown in **Figure S6**. A peak at retention time of 18.2 min was ascribed to pentamethylcyclopentadiene(PMCP).

As shown in **Figure S7**, under relatively higher temperature of 400 °C, in which full methanol conversion was realized, we can still successfully capture $PMCP^+$ cations and neutral PMCP.

The ^{13}C MAS NMR spectra presenting the variation of confined organics with time on-stream are shown in **Figure S8a**, and the concentrations of $PMCP^+$ were quantitatively calculated according to the integral area of the ring carbon atoms with the characteristic peaks at 240-250 ppm[10-11]. The concentration evolutions of $PMCP^+$ with time on-stream (TOS) is displayed in **Figure S8b.** The concentration evolving trend of $PMCP^+$ with TOS (Figure S8b) are almost consistent with the methanol conversion profile (**Figure S4**) throughout the MTO reaction, except that the maximum concentration was around 10 minutes delay of highest methanol conversion.

The GC-MS chromatograms providing the variation of confined organics with time on-stream are shown in **Figure S9a**, and the concentrations of PMCP were quantitatively calculated according to the area of the peak at retention time of 18.20 min taking C_2Cl_6 as internal standard. The concentration evolutions of PMCP with time on-stream (TOS) is displayed in **Figure S9b.** Likewise, the concentration evolutions of PMCP with TOS (**Figure S9b**) approximately accord with the corresponding cations ($PMCP^+$) (**Figure S8b**) and methanol conversion profile (Figure S4). Moreover, as shown in **Figure S9b**, the concentration comparison of hexaMB and PMCP (quantitatively calculated according to the area of the corresponding peaks in **Figure S9a**) show that PMCP has similar varying trend with hexaMB, though hexaMB exhibits higher concentration than PMCP.

UV-vis spectra after MTO reaction for different durations were also applied to trace the evolution of active intermediates as shown in **Figure S10**. In addition, UV-vis spectra after MTO reaction for different durations were also applied to trace the evolution of active intermediates (**Figure S10**). The band centered at 275 nm has combined contributions from polyalkyl-substituted cyclopentadienium ions as well as from neutral and cationic methylbenzenes. The band at 295 nm can be assigned to the polyalkyl-substituted cyclopentadienium ions.[12] The absorption band at 354 nm is representative of the methylbenzenium ions. Likewise, absorption intensity with TOS is in agreement with the methanol conversion profile (**Figure S4**).
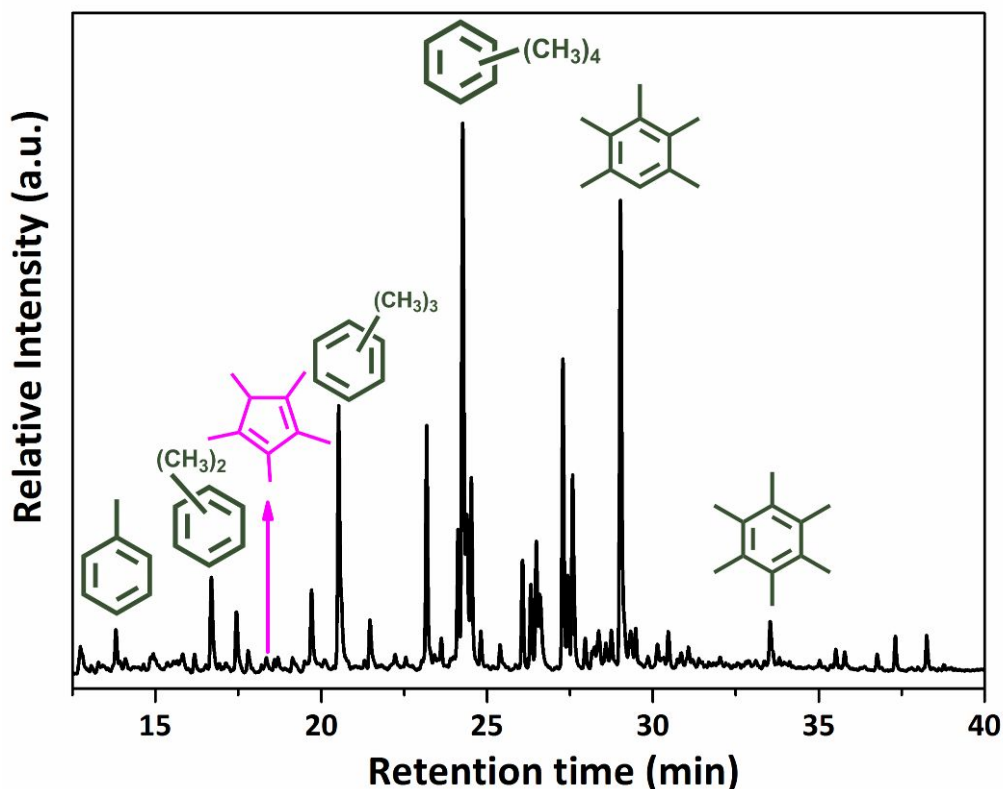

Figure S6. GC-MS chromatograms of the organic species retained in H-SAPO-34 catalyst after CH_3OH conversion at 300 °C for 25 min. WHSV of CH_3OH = 2.0 h^{-1}.
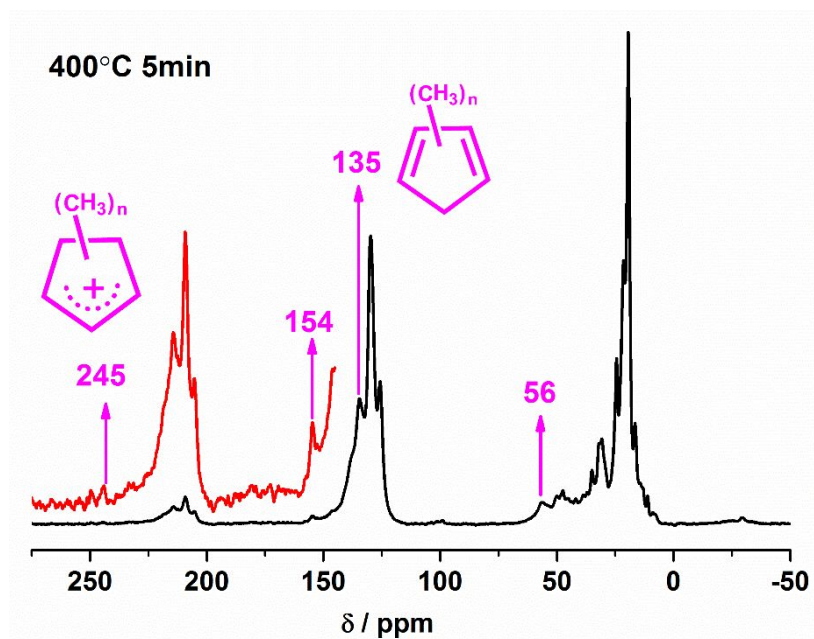
Figure S7. ^{13}C MAS NMR spectra of the organic intermediates retained in H-SAPO-34 after continuous flow $^{13}CH_3OH$ reaction at 400 °C for 5 min.

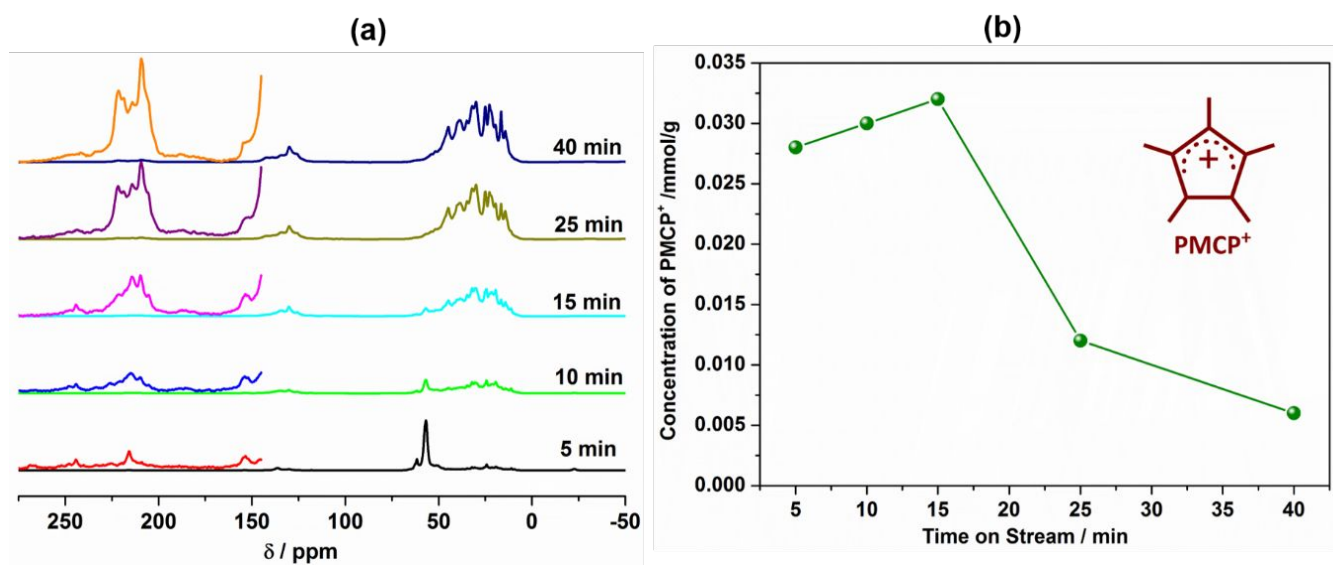**Figure S8.** (a) ^{13}C MAS NMR spectra of $^{13}CH_3OH$ reaction on H-SAPO-34 with time on-stream under continuous-flow condition at 300 °C. (b) The concentrations of PMCP+ with time on-stream.
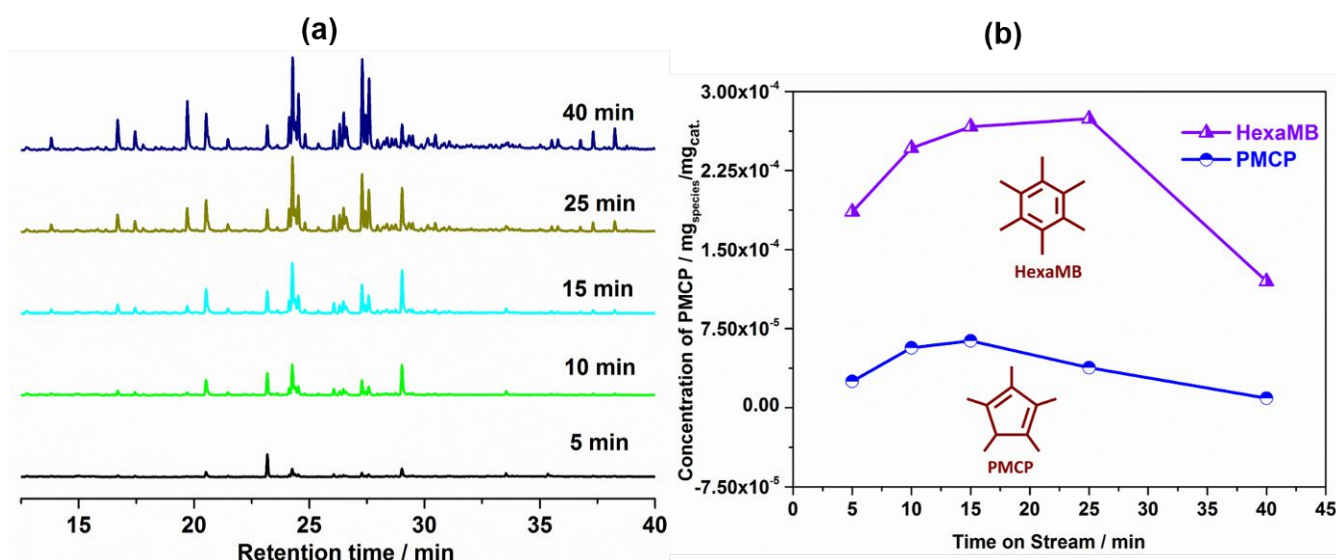
Figure S9. (a) GC-MS chromatograms of the organic species retained in H-SAPO-34 catalyst with time on-stream at 300 °C. (b) The concentrations of PMCP (mg$_{species}$/mg$_{cat.}$) were quantitatively calculated according to the area of the peak at retention time of 18.2 min taking C_2Cl_6 as internal standard.
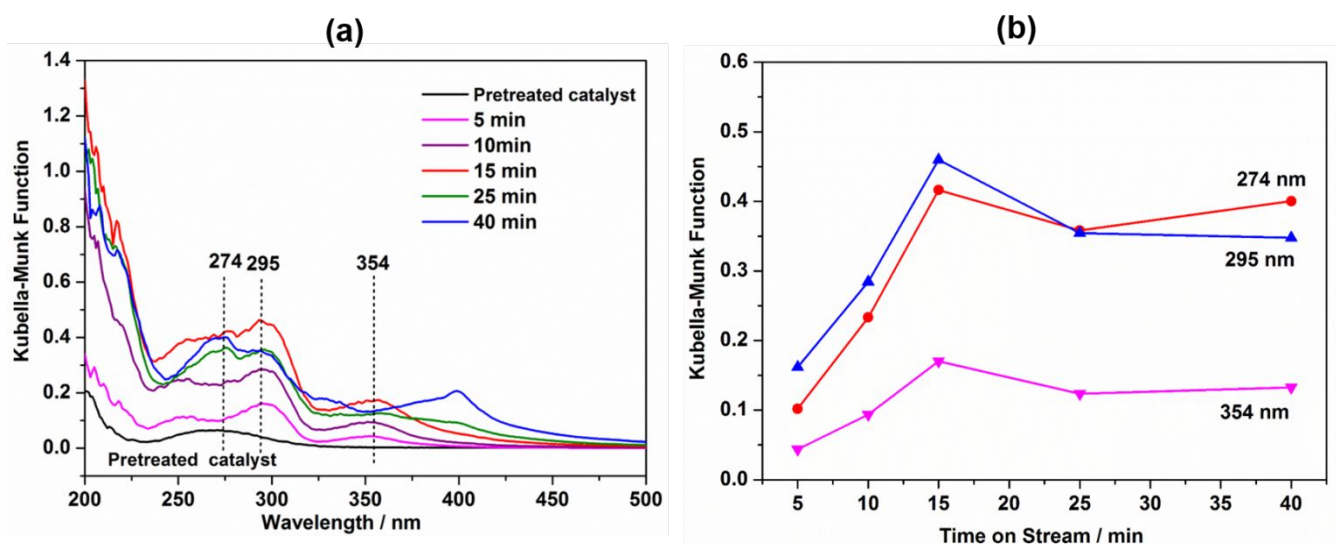

Figure S10. (a) The diffuse reflectance of ex-situ UV-vis spectra after methanol conversion for different durations at 300 °C. (b) Absorption intensity of various wavelengths with time on-stream.

3.3 Cyclopentadienes-based Cycle Starting from PMCP⁺

The Gibbs free energy barrier, the enthalpic and entropic contributions and reaction rate constant for all reaction steps at 400 °C are provided in **Table S1**.

Optimized transition state structures of all the elements for olefins formation via the cyclopentadienes-based cycle starting from PMCP⁺ are shown in **Figure S11**.

The optimized transition state structures for the ethene and propene precursors (methylcyclopentenyl cation with ethyl or propyl side-chain) formations are shown in **Figure S12**.

Table S1. Calculated free energy barriers ($\Delta G^{\ddagger}$), the enthalpic and entropic contributions and reaction rate constant at 400 °C for olefins formation via the cyclopentadienes-based cycle starting from PMCP$^+$ in MTO over H-SAPO-34.

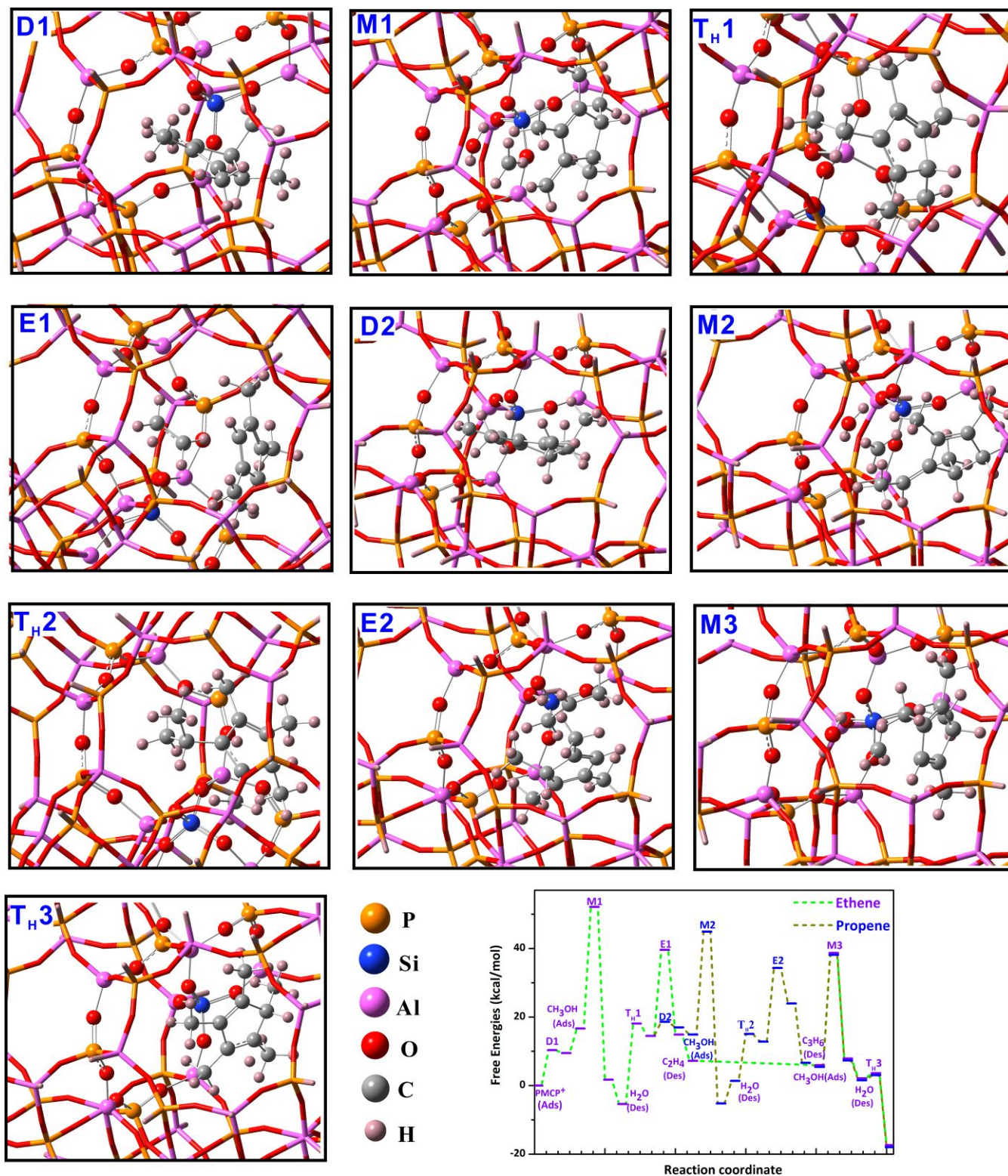| Olefins Formation Based on PMCP$^+$			
Reactions	$\Delta G^{\ddagger}$ (kcal/mol)	$\Delta H^{\ddagger}$ (kcal/mol)	$-T\Delta S^{\ddagger}$ (kcal/mol)	k (s^{-1})
D1	10.34	7.20	3.14	5.93×10^{7}
M1	35.47	29.05	6.42	3.89×10^{1}
T_H1	23.48	22.13	1.35	8.22×10^{4}
E1	25.10	28.06	-2.96	9.92×10^{3}
D2	4.10	3.03	1.07	4.27×10^{9}
M2	30.02	26.12	3.90	1.71×10^{3}
T_H2	13.75	16.70	-2.95	5.53×10^{7}
E2	21.47	21.73	-0.26	7.91×10^{4}
M3	32.74	29.60	3.14	1.60×10^{2}
T_H3	1.51	0.18	1.33	3.11×10^{12}

Figure S11. Optimized transition state structures of all the elementary reactions for olefins formation via the cyclopentadienes-based cycle starting from PMCP$^+$.
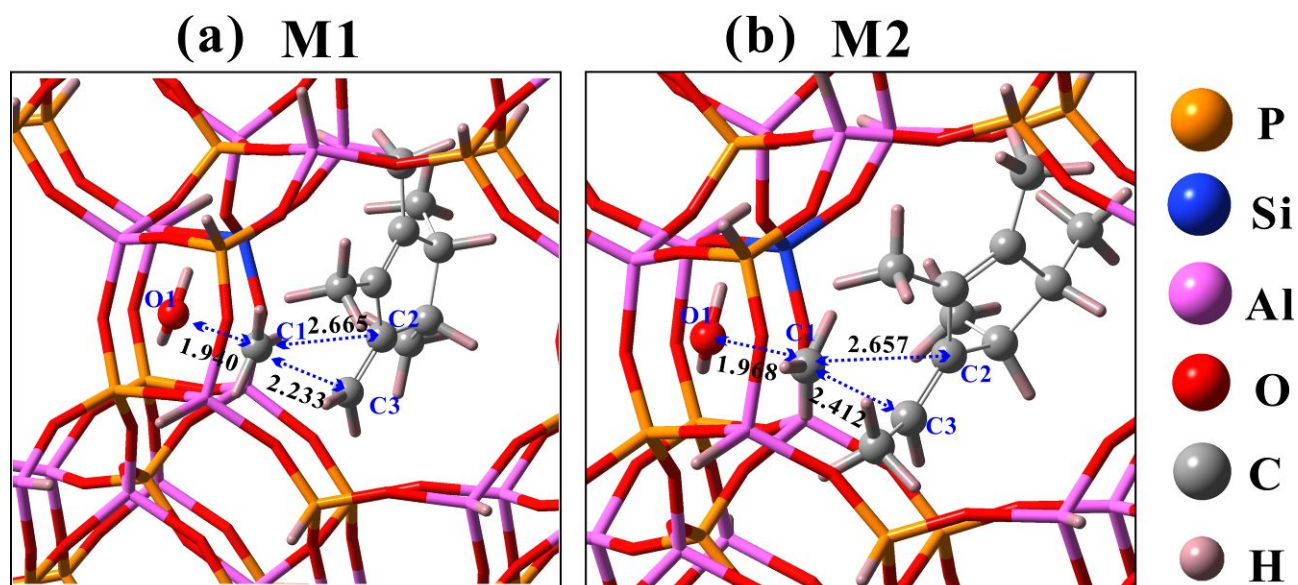
Figure S12. Optimized transition state structures for the formations of cyclopentenyl cation with alkyl side-chain. TMECP+ (2, 3, 4, 5-tetraM-1-ECP+, **M1**) (a) and TMPCP+ (2, 3, 4, 5-tetraM-1-PCP+, **M2**) (b) as the precursors for ethene and propene formation.
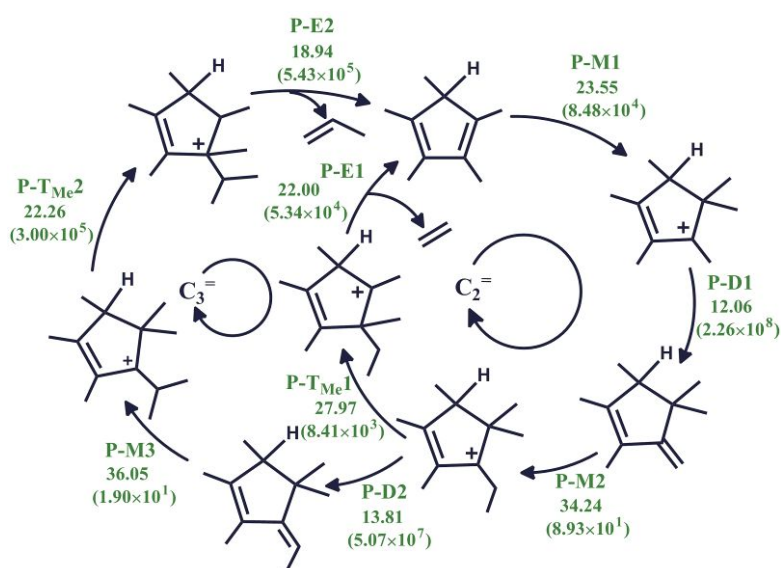
Table S2. Calculated free energy barriers ($\Delta G^{\ddagger}$), the enthalpic and entropic contributions and reaction rate constant at 300 °C for olefins formation via the cyclopentadienes-based cycle starting from PMCP+ cycle in MTO over H-SAPO-34.

	Olefins Formation Based on PMCP+			
Reactions	$\Delta G^{\ddagger}$ (kcal/mol)	$\Delta H^{\ddagger}$ (kcal/mol)	$-T\Delta S^{\ddagger}$ (kcal/mol)	k (s^{-1})
D1	9.88	7.28	2.6	8.73×10^6
M1	35.52	29.13	6.39	7.32×10^{-1}
T_H1	23.29	22.26	1.03	3.03×10^3
E1	25.54	28.11	-2.57	1.45×10^2
D2	3.94	3.11	0.83	1.01×10^9
M2	29.45	26.17	3.28	4.51×10^1
T_H2	14.19	16.80	-2.61	3.63×10^6
E2	21.51	21.76	-0.25	2.36×10^3
M3	32.27	29.61	2.66	2.53×10^0
TH3	1.33	0.38	0.95	2.41×10^{12}

3.4 Cyclopentadienes-based Cycle Starting from PMCP

The cycle starts from the gem-methylation of PMCP as shown in **Scheme S1**. The energy profiles of ethene

and propene formation are shown in **Figure S13**. The free energy barriers, the enthalpic and entropic contributions and reaction rate constants for all reaction steps at 400 °C are provided in **Table S3**.

Scheme S1. Cyclopentadienes-based cycle, the proposed mechanism for ethene and propene formation starting from PMCP in H-SAPO-34. Calculated free energy barriers and reaction rate constants (in brackets) at 400 °C are given in kcal/mol and s^{-1}.

Table S3. Calculated free energy barriers ($\Delta G^{\ddagger}$), the enthalpic and entropic contributions and reaction rate constant at 400 °C for olefins formation via the cyclopentadienes-based cycle starting from PMCP cycle in MTO over H-SAPO-34.

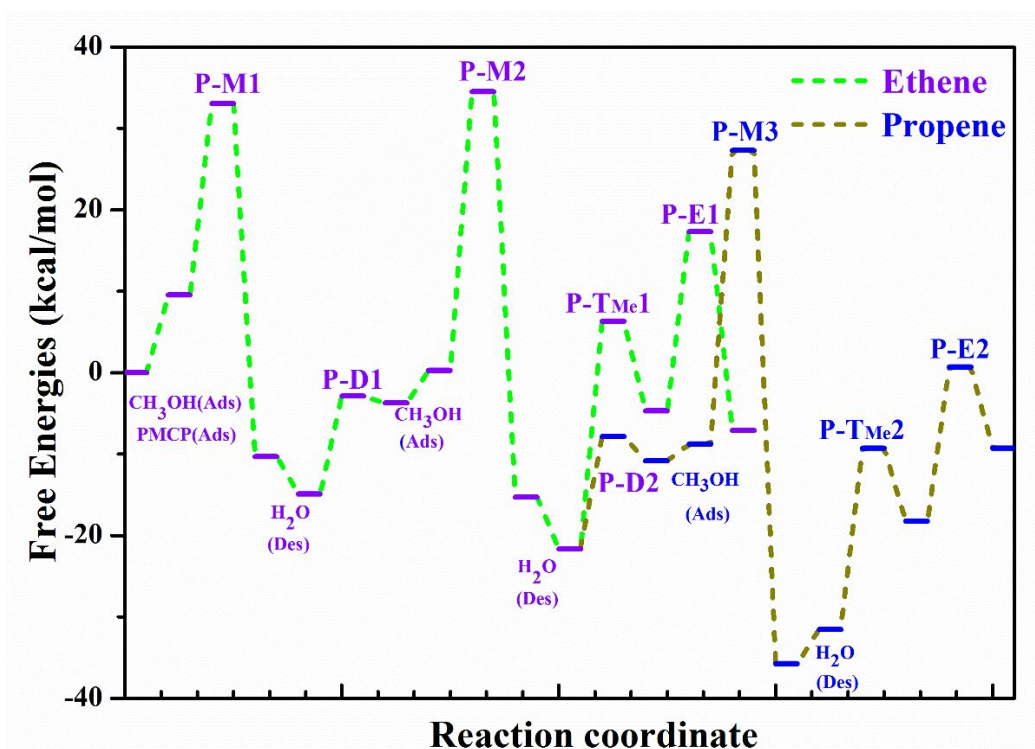| Olefins Formation Based on PMCP				
Reactions	$\Delta G^{\ddagger}$ (kcal/mol)	$\Delta H^{\ddagger}$ (kcal/mol)	$-T\Delta S^{\ddagger}$ (kcal/mol)	k (s^{-1})
P-M1	23.55	22.98	0.57	8.48×10^4
P-D1	12.06	7.36	4.70	2.26×10^8
P-M2	34.24	29.42	4.82	8.93×10^1
P-T$_{Me}$1	27.97	24.27	3.27	8.41×10^3
P-E1	22.00	27.04	-5.04	5.34×10^4
P-D2	13.81	10.30	3.51	5.07×10^7
P-M3	36.05	34.57	1.47	1.90×10^1
P-T$_{Me}$2	22.26	20.67	1.59	3.00×10^5
P-E2	18.94	18.43	0.51	5.43×10^5

Figure S13. Gibbs free energy profiles of the ethene and propene formations over H-SAPO-34 following the cyclopentadienes-based route staring from PMCP.

3.5 Comparisons and Interconversion between Active Intermediates of Indirect Mechanism

The free energy barriers at 300 ^{o}C for ethene and propene precursors formations via various reaction routes on H-SAPO-34 is listed in **Table S4.**
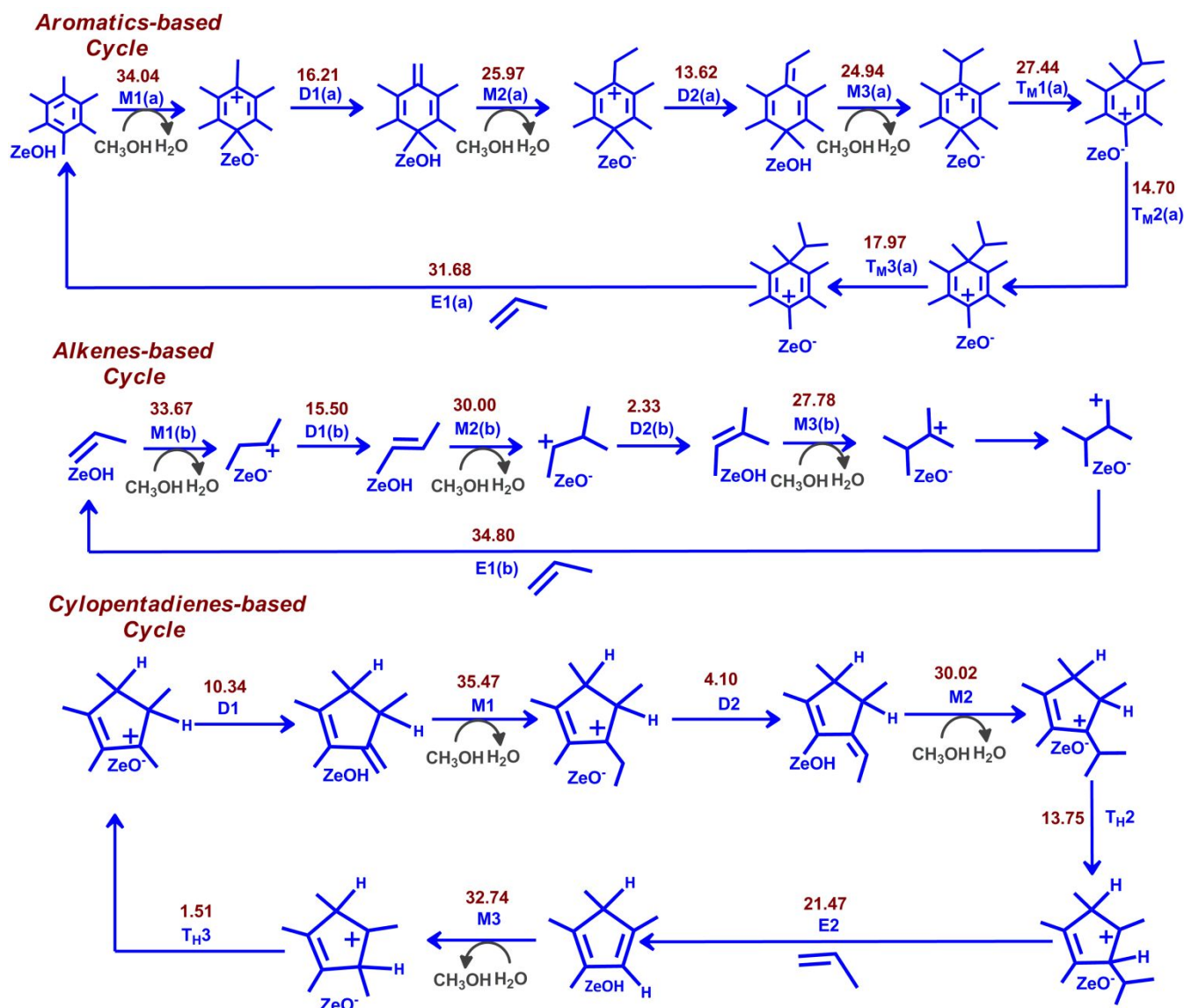
The mechanism routes and free energy barriers based on aromatics-based (side-chain mechanism), alkenes-based and our proposed cyclopentadienes-based cycle for propene formation over H-SAPO-34 are displayed in **Scheme S2**.

The conversion of PMCP$^+$ to tetramethylbenzene linking cyclopentadienes-based and aromatics-based cycle on H-SAPO-34 is examined in **Scheme S3.**
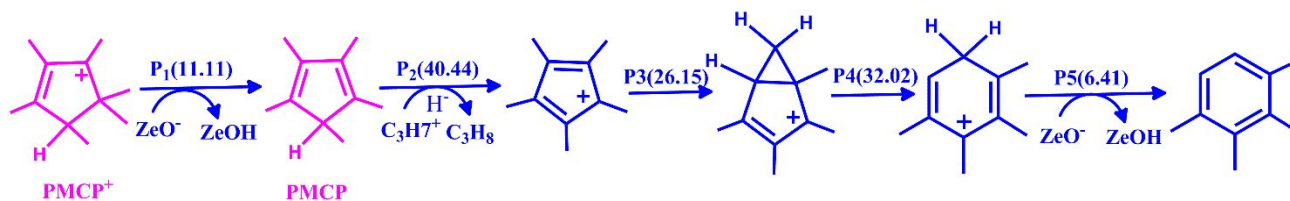
The interconversion between active intermediates and their interdependent correlations in the catalytic cycles is shown in **Scheme S4.**

Table S4. Calculated free energy barriers (ΔG‡, kcal/mol) at 300 ^{o}C for ethene and propene precursors formations via various reaction routes on H-SAPO-34 (Alkenes-based, Aromatics-based and Cy-clopentadienes-based catalytic cycles).

ΔG‡(kcal/mol) Reactions	Alkenes-based Cycle	Aromatics-based Cycle	Cyclopentadienes-based Cycle
Ethene Precursor	37.44	25.50	35.52
Propene Precursor	32.90	24.64	29.45

15

Scheme S2. The mechanism routes based on aromatics-based (side-chain mechanism), alkenes-based and our proposed cyclopentadienes-based cycle for propene formation over H-SAPO-34. Free energy barriers in kcal/mol at 400 °C are displayed. Reaction types: D (deprotonation), M (methylation), T_H (Hydride-transfer), T_M(Methyl-transfer), E (elimination).

Scheme S3. The conversion of PMCP$^+$ to tetramethylbenzene linking cyclopentadienes-based and aromatics-based cycle over H-SAPO-34. Free energy barriers in kcal/mol at 400 °C are displayed in brackets.
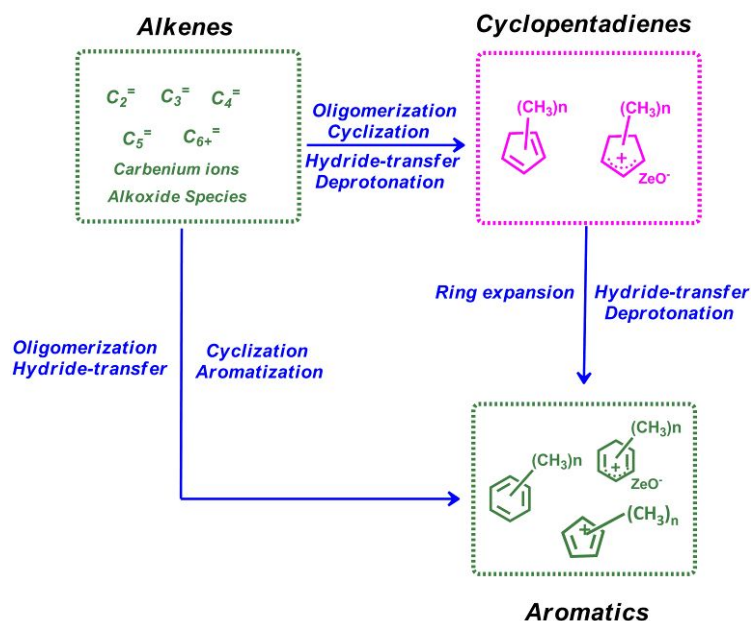
Scheme S4. The interconversion between active intermediates and their interdependent correlations in the catalytic cycles.

Reference

(1) Chen, J.; Li, J.; Wei, Y.; Yuan, C.; Li, B.; Xu, S.; Zhou, Y.; Wang, J.; Zhang, M.; Liu, Z., Spatial confinement effects of cage-type SAPO molecular sieves on product distribution and coke formation in methanol-to-olefin reaction. *Catal. Commun.* **2014,** *46*, 36-40.

(2) Guisnet, M.; Costa, L.; Ribeiro, F. R., Prevention of zeolite deactivation by coking. *J. Mol. Catal. A: Chem.* **2009,** *305*, 69-83.

(3) O'Malley, P. J.; J., D., Ab-initio molecular orbital calculations on the siting of aluminium in the Theta-1 framework: Some general guidelines governing the site preferences of aluminium in zeolites. *Zeolites* **1988,** *8*, 317-321.

(4) Chu, Y.; Han, B.; Zheng, A.; Deng, F., Influence of Acid Strength and Confinement Effect on the Ethylene Dimerization Reaction over Solid Acid Catalysts: A Theoretical Calculation Study. *J. Phys. Chem. C.* **2012,** *116*, 12687-12695.

(5) Lesthaeghe, D.; De Sterck, B.; Van Speybroeck, V.; Marin, G. B.; Waroquier, M., Zeolite shape-selectivity in the gem-methylation of aromatic hydrocarbons. *Angew. Chem., Int. Ed.* **2007,** *46*, 1311-1314.

(6) Papayannis, D. K.; Papavasileiou, K. D.; Melissas, V. S., Investigation of bromine atom transfer mechanism from an alkyl bromide molecule to an O-bonded alkyl group in a FAU zeolite by the ONIOM method. *Microporous Mesoporous Mater.* **2016,** *226*, 1-9.

(7) Chai, J. D.; Head-Gordon, M., Long-range corrected hybrid density functionals with damped atom-atom dispersion corrections. *Phys. Chem. Chem. Phys.* **2008,** *10*, 6615-6620.

(8) Frisch, M. J.; Trucks, G. W.; Schlegel, H. B.; Scuseria, G. E.; Robb, M. A.; Cheeseman, J. R.; Scalmani, G.; Barone, V.; Mennucci, B.; Petersson, G. A.; Nakatsuji, H.; Caricato, M.; Li, X.; Hratchian, H. P.; Izmaylov, A. F.; Bloino, J.; Zheng, G.; Sonnenberg, J. L.; Hada, M.; Ehara, M.; Toyota, K.; Fukuda, R.; Hasegawa, J.; Ishida, M.; Nakajima, T.; Honda, Y.; Kitao, O.; Naka, H.; Vreven, T.; Montgomery, J. A.; Peralta, J. E.; Ogliaro, F.; Bearpark, M.; Heyd, J. J.; Brothers, E.; Kudin, K. N.; Staroverov, V. N.; Kobayashi, R.; Normand, J.; Raghavachari, K.; Rendell, A.; J. Burant, C.; Iyengar, S. S.; Tomasi, J.; Cossi,;M.; Rega, N.; Millam, J. M.; Klene, M.; Knox, J. E.;

Cross, J. B.; Bakken, V.; Adamo, C.; Jaramillo, J.; Gomperts, R.; Stratmann, R. E.; Yazyev, O.; Austin, A. J.; Cammi, R.; Pomelli, C.; Ochterski, J. W.; Martin, R. L.; Morokuma, K.; Zakrzewski, V. G.; Voth, G. A.; Salvador, P.; Dannenberg, J. J.; Dapprich, S.; Daniels, A.D.; Farkas, O.; Foresman, J. B.; V.Ortiz, J.; Cioslowski, J.; Fox, D. J. Gaussian 09, Revision B.01, Gaussian, Inc.: Wallingford, CT, **2010**.

(9) Ghysels, A. V., T.; Hemelsoet, K.; Waroquier, M.; Van Speybroeck, V., TAMkin :A Versatile Package for Vibrational Analysis and Chemical Kinetics. *J. Chem. Inf. Model.* **2010,** *50*, 1736-1750.

(10) Xu, S.; Zheng, A.; Wei, Y.; Chen, J.; Li, J.; Chu, Y.; Zhang, M.; Wang, Q.; Zhou, Y.; Wang, J.; Deng, F.; Liu, Z., Direct Observation of Cyclic Carbenium Ions and Their Role in the Catalytic Cycle of the Methanol-to-Olefin Reaction over Chabazite Zeolites. *Angew. Chem., Int. Ed.* **2013,** *52*, 11564-11568.

(11) Haw, J. F.; Nicholas, J. B.; Song, W. G.; Deng, F.; Wang, Z. K.; Xu, T.; Heneghan, C. S., Roles for cyclopentenyl cations in the synthesis of hydrocarbons from methanol on zeolite catalyst HZSM-5. *J. Am. Chem. Soc.* **2000,** *122*, 4763-4775.

(12) Wulfers, M. J.; Jentoft, F. C., The Role of Cyclopentadienium Ions in Methanol-to-Hydrocarbons Chemistry. *ACS. Catal.* **2014,** *4*, 3521-3532.